Bio-Signal Controlled Exoskeleton for Accurate Elbow Rehabilitation

Wang Ziyi *

Hainan Haidian Foreign Language Shi Yan School (HFLSS), Qionghai, Hainan Province, China

* Corresponding Author Email: 10673976@qq.com

Abstract. To address the limitations of current elbow rehabilitation exoskeletons—namely insufficient force-control accuracy, low active user engagement, and poor adaptability to individual needs—this work develops a precision-controlled exoskeleton system based on biological signal perception. The system acquires muscle activity through surface electromyography (sEMG) sensors and identifies movement intentions using a convolutional neural network (CNN). A differential transmission mechanism is employed to drive elbow flexion–extension and forearm pronation–supination, enabling two degrees of freedom. Experiments were conducted with four healthy subjects to compare sEMG signals (RMS) and primary joint torque between a free mode and an assistive mode under three forearm postures (neutral, pronation, and supination). Results show that, in assistive mode, the RMS of major upper-limb muscles decreased by an average of 38.53 ± 11.98%, and primary joint torque decreased by an average of 58.5 ± 17.27%. The brachioradialis exhibited the largest RMS reduction in the neutral posture (54.76 ± 16.69%), while the supination posture resulted in the greatest torque reduction (66.2 ± 15.34%). These findings demonstrate that the proposed system effectively reduces muscle activation and voluntary effort, validating its effectiveness in rehabilitation training and the stability of human–robot cooperative control.

Keywords: Elbow exoskeleton; Electromyography (EMG); Movement intention recognition; Convolutional neural network (CNN); Assistive control; Rehabilitation training.

1. Introduction

Upper-limb motor impairment is a common clinical condition that severely affects patients' quality of life, with epidemiological studies showing significant disease burden and social impact [1, 2]. As a key biomechanical pivot connecting the shoulder and the hand, the elbow joint plays a critical role in the upper-limb kinetic chain. Elbow injuries are frequent, and rehabilitation often relies on plaster immobilization followed by natural recovery (Figure 1). However, prolonged immobilization leads to muscle inactivity, which can negatively affect muscles, bones, joints, and ligaments, potentially causing muscle atrophy, strength loss, osteoporosis, joint stiffness, fibrotic adhesion, and ligament fragility [3, 4]. To improve rehabilitation outcomes and shorten recovery time, this study develops a rehabilitation exoskeleton device specifically designed for elbow joint injuries.

Conventional rehabilitation, such as therapist-guided manual training, is limited by scarce clinical resources and difficulty in precisely controlling training intensity. Rehabilitation robots and exoskeletons have thus emerged as effective alternatives. These systems generally fall into two categories: end-effector–based and exoskeleton-based robots, each with distinct advantages in clinical applications. End-effector systems are particularly suitable for passive training in the early recovery stage, whereas exoskeleton-type robots, due to their wearable characteristics, are better suited for personalized rehabilitation tailored to individual patient needs [5–7]. Recent advances in sensing and control algorithms have significantly improved the motion accuracy and adaptability of exoskeleton robots. For example, Ref. [8] introduced a 5-DOF upper-limb exoskeleton using an improved D–H algorithm, capable of accurately decoding user intention and providing real-time assistance, thereby enhancing the specificity of rehabilitation training and improving user engagement.

In recent years, bio-signal–based human–machine interface technologies—such as surface electromyography (sEMG) and electroencephalography (EEG)—have shown great potential for upper-limb rehabilitation in stroke patients. Non-invasive brain–computer interface (BCI) systems decode neural-muscular activity or movement intention and integrate with virtual reality (VR), functional electrical stimulation (FES), and robotic exoskeletons to promote motor function recovery [9, 10]. Motor-imagery–based BCI training can enhance cortical excitability on the affected side, facilitate functional reorganization of motor-related brain regions, and ultimately improve upper-limb motor performance (e.g., increased Fugl–Meyer scores) and daily living ability (e.g., improved Modified Barthel Index) [11, 12]. Additionally, BCI systems combined with mirror therapy can strengthen the association between motor intention and actual limb movement through enhanced visual feedback, further improving rehabilitation efficacy. Such systems not only yield functional improvements but also modulate serum neurotrophic factors (e.g., brain-derived neurotrophic factor, BDNF), promoting neural plasticity [13].

Despite the progress in elbow rehabilitation exoskeletons, several critical challenges remain unresolved. Existing systems generally exhibit three major limitations:

1) Insufficient force-control accuracy—most devices rely on preset trajectories or simple impedance control, making them unable to adapt to real-time variations in user muscle strength. This often leads to inaccurate assistance or even counteracting forces that compromise rehabilitation effectiveness.

2) Limited active training mechanisms—conventional devices focus primarily on passive motion and lack real-time intention detection and feedback, resulting in low patient engagement and suboptimal neuroplasticity training outcomes.

3) Poor adaptability to individual differences—many systems have restricted mechanical adjustability and rigid control architectures (e.g., the bulky exoskeleton shown in Figure 2), making it difficult to accommodate variations in anatomy (e.g., forearm length, joint mobility) and rehabilitation-stage requirements.

To address these issues, this work presents a biologically informed, intention-driven elbow exoskeleton rehabilitation system. By sensing biological signals and predicting user movement intention, the system enables precise and compliant assistive control. It supports elbow flexion–extension as well as forearm pronation–supination, providing comprehensive training for individuals with elbow joint injuries and promoting early functional recovery. Compared with existing devices, the proposed system offers significant improvements in force-control precision, active user engagement, and adaptability, providing a smarter and more effective rehabilitation solution with strong clinical application potential.

Figure 1. Plaster splint fixation for an injured elbow

Figure 2. A bulky exoskeleton device

2. Human Elbow Joint Anatomical Analysis

2.1. Overview of the Human Elbow Joint

As a key pivot in the upper-limb kinetic chain, the elbow joint possesses a highly refined and complex anatomical structure formed by multiple articulations working synergistically to enable coordinated motion. As illustrated in Figure 3, the elbow joint is primarily composed of four interconnected joints:

1) Humeroulnar joint—the main weight-bearing articulation, consisting of the trochlear notch of the ulna articulating with the humeral trochlea to form a precise hinge mechanism;

2) Humeroradial joint—formed by the capitulum of the humerus and the radial head, participating not only in flexion–extension but also contributing to forearm rotation;

3) Proximal radioulnar joint—constituted by the annular articular surface of the radius and the ulna;

4) Distal radioulnar joint—formed by the ulnar articular surface and the ulnar notch of the radius together with the triangular fibrocartilage complex (TFCC).

The proximal and distal radioulnar joints work in concert to achieve forearm pronation–supination. Under the combined constraint of ligaments, muscles (see Figure 4), and the joint capsule, these articulations maintain a balance between mobility and stability, ensuring smooth and controlled upper-limb movement.

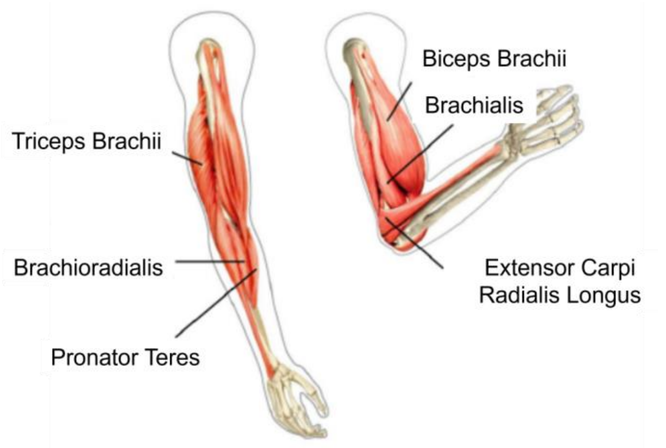

Figure 3. Skeletal structure of the elbow and forearm

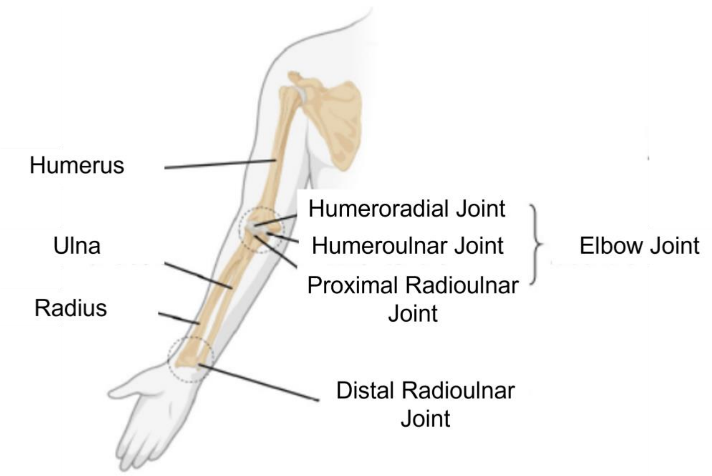

Figure 4. Muscular distribution of the elbow and forearm

2.2. Elbow and Forearm Motion Analysis

The primary functions of the elbow joint involve flexion–extension and forearm rotation. As shown in Figure 5, the normal elbow exhibits a flexion–extension range from 0° (full extension) to 145° (full flexion), and some individuals may demonstrate slight hyperextension of approximately -5° to 0°. Elbow flexion is primarily driven by the brachialis, biceps brachii, and brachioradialis, while extension is dominated by the triceps brachii and anconeus.

In terms of forearm rotation (Figure 6), the pronation range is typically 0°~75° (rotation of the palm downward), actuated by the pronator teres and pronator quadratus. Supination ranges from 0°~85° (palm turning upward), controlled mainly by the supinator and the biceps brachii.

For safety and practicality in exoskeleton design, the motion range is intentionally set slightly below the physiological limits. As summarized in Table 1, the exoskeleton's elbow flexion range is designed as 0°~125°, lower than the physiological 145°. Forearm pronation and supination are designed as 0°~70° each, also moderately constrained relative to natural motion. Hyperextension of the elbow is completely restricted (0°~0°) to ensure joint stability. This design strategy preserves training effectiveness while minimizing the risk of injury due to excessive movement.

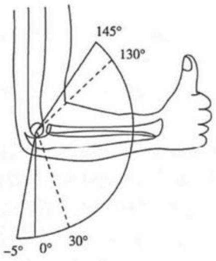

Figure. 5 Range of elbow flexion–extension

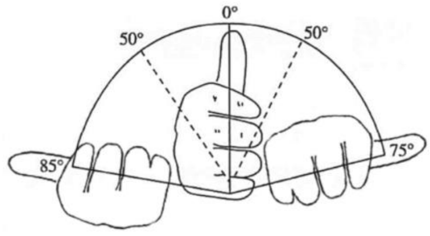

Figure. 6 Range of forearm pronation–supination

Table 1 Exoskeleton Design Motion Range [14]

Joint Motion	Physiological Range	Exoskeleton Design Range	Primary Muscles Involved
Elbow flexion	0°~145°	0°~125°	Brachialis, Biceps brachii, Brachioradialis
Elbow extension	-5°~0°	0°~0°	Triceps brachii, Anconeus
Forearm pronation	0°~75°	0°~70°	Pronator teres, Pronator quadratus
Forearm supination	-85°~0°	-70°~0°	Supinator, Biceps brachii

3. System Design

The exoskeleton device consists of a mechanical structure and a control system. From an anatomical perspective, the elbow is a typical hinge joint, with motion primarily regulated by the humeroulnar and humeroradial articulations. Forearm rotation is coordinated through the proximal and distal radioulnar joints, forming a compound system capable of both flexion–extension and pronation–supination.

At the signal acquisition level, sEMG sensors are positioned according to international standards to record activity from major muscles, including the biceps brachii and triceps brachii. The signals undergo wavelet-based denoising and time–frequency feature extraction, which are then used to build an artificial neural network model for joint-angle prediction.

The control system employs a CAN bus protocol to transmit predicted torque values in real time to the exoskeleton's actuation units. Feedback from motor encoders, combined with real-time positional data calculated via a biomechanical moment-arm model, forms a closed-loop control strategy integrating both feedforward and feedback elements. This enables an intelligent assistive system that combines sEMG-based feedforward control with position-based feedback correction, providing precise and adaptive support during rehabilitation.

3.1. Mechanical Structure Design

The exoskeleton system adopts a modular design (Figure 7) and is mainly composed of three subsystems: the motion execution system, the transmission system, and the control system. The motion execution system includes a serially arranged elbow rotation module and a differential actuation module, responsible for driving elbow flexion–extension and forearm pronation–supination, respectively.

The transmission system employs a tendon-driven distal actuation scheme, with motors and other power units housed externally in an independent control cabinet. Motion is transmitted via flexible tendons, reducing the weight borne by the wearer.

The control system integrates multi-channel data acquisition and real-time processing capabilities, enabling programmable execution of various rehabilitation training modes. This design effectively reduces the overall system weight, enhances wearing comfort, and improves motion-control precision. By optimizing structural compactness and human–machine interaction safety, it provides stable and efficient hardware support for rehabilitation training.

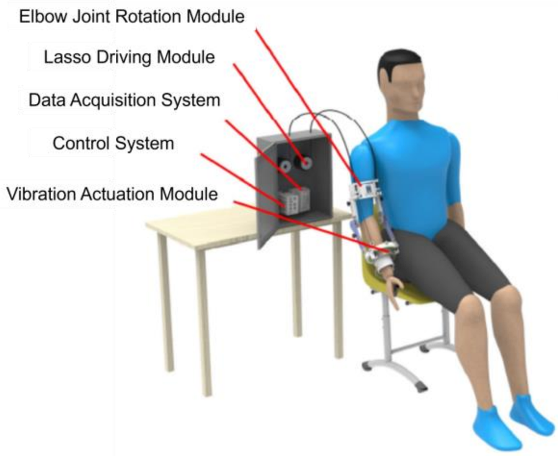

Figure. 7 Schematic diagram of the exoskeleton system

Figure 8 illustrates the elbow rotation module. The exoskeleton system achieves two degrees of freedom through coordinated dual-motor control: during elbow flexion–extension, both motors rotate in the same direction at equal speed, generating tendon tension that balances torque around the forearm’s central axis (Y-axis) while producing a net torque around the elbow rotation axis (X-axis). During forearm rotation, the motors rotate in opposite directions at equal speed, canceling torques around the X-axis and generating net torque along the Y-axis. This differential transmission mechanism, enabled by coordinated motor control, decouples the two degrees of freedom, ensuring precise and stable motion output. Figure 9 shows the actual elbow joint device.

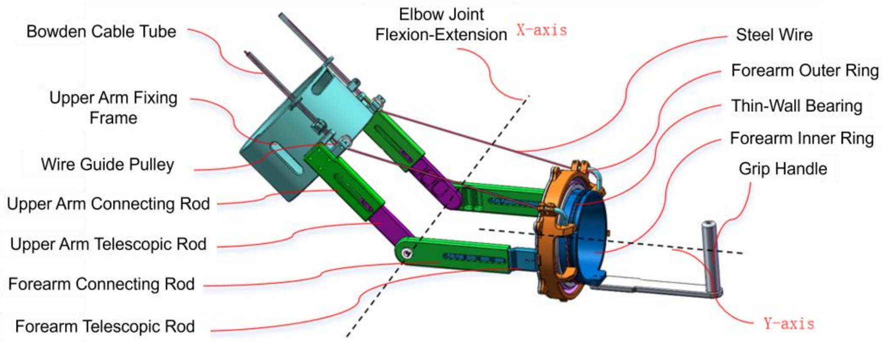

Figure. 8 Schematic diagram of the elbow rotation module

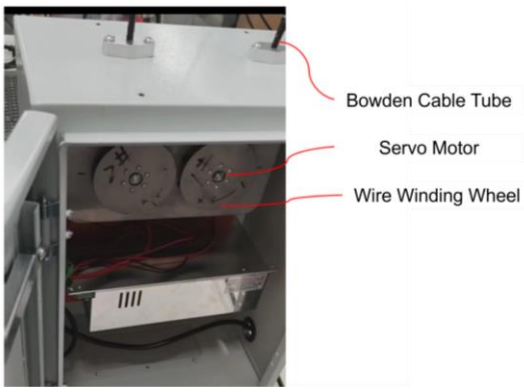

Figure. 9 Elbow joint device

3.2. Control System Design

As shown in Figure 10, the control system employs a distributed architecture consisting of a host PC and a motion control card, with real-time communication implemented via a CAN bus. sEMG signals collected by the sensors are transmitted to the motion control module through a USB interface. After signal processing and movement intention decoding, control commands are generated and sent as pulse/direction signals to drive the servo motors, enabling precise control of the exoskeleton's actuation system. This architecture combines real-time performance with scalability, providing a hardware foundation for multimodal signal integration and dynamic adjustment of rehabilitation strategies.

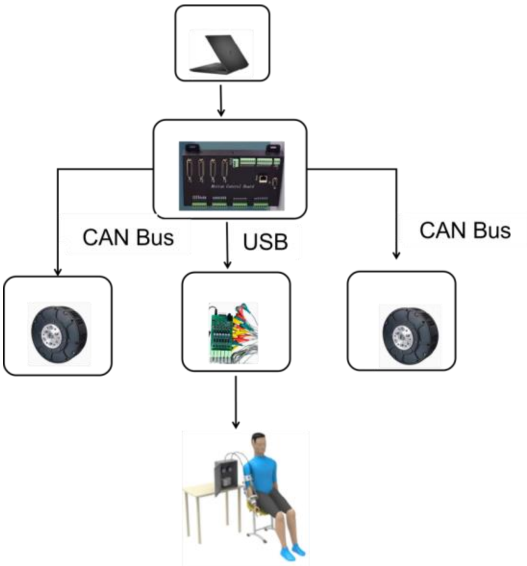

Figure. 10 Components of the elbow exoskeleton system

As shown in Figures 11 and 12, the system uses sEMG sensors to detect movement intention, with the receiver module working in coordination with wearable electrodes. EMG signals originate from motor neuron action potentials triggering the release of acetylcholine at neuromuscular junctions, causing changes in muscle cell membrane potential. When the potential exceeds a threshold, muscle fiber action potentials propagate along the membrane, inducing muscle contraction via the excitation–contraction coupling mechanism.

Surface electrodes capture the microvolt-level potential differences generated on the skin by this electrical activity. After amplification, filtering, and analog-to-digital conversion, these bioelectrical signals are transformed into quantifiable digital signals for processing. This sensing system provides highly sensitive physiological inputs for exoskeleton control and is a critical component for achieving human–robot cooperative motion.

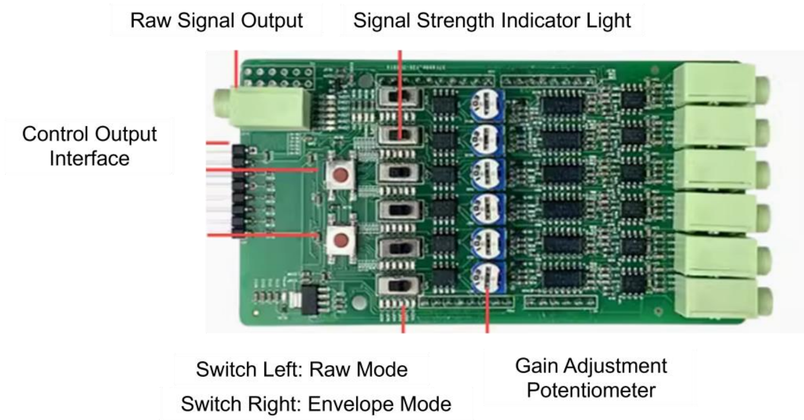

Figure. 11 EMG sensor receiver

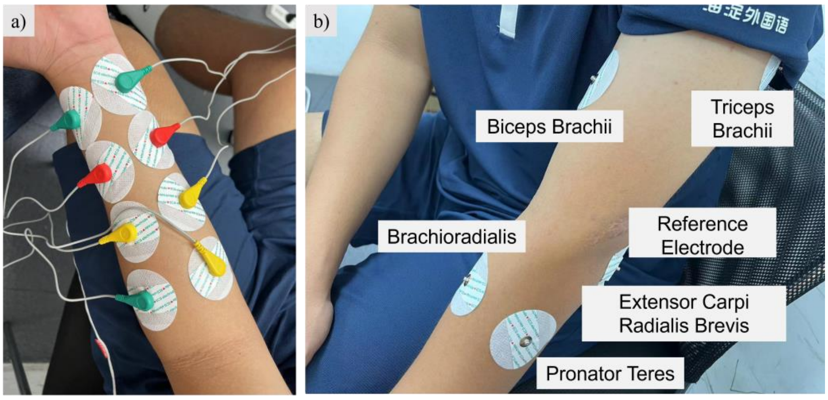

Figure. 12 Placement of EMG sensor electrodes: (a) electrode positions on the forearm; (b)electrode positions on the upper arm and corresponding muscle groups

3.3. Algorithm Design

To accurately decode human movement intention for the exoskeleton system, this study uses sEMG signals as the input to the control system and establishes an elbow joint motion prediction model through signal processing and intelligent algorithms. This approach leverages the bioelectrical–mechanical coupling between EMG signals and joint motion. After feature extraction and pattern recognition, it enables real-time assessment of elbow joint motion, providing decision support for exoskeleton control.

The raw sEMG signals undergo band-pass filtering, full-wave rectification, and sliding-window averaging before being fed into a convolutional neural network (CNN) for feature extraction and motion mapping. As shown in Figure 13, the CNN model employs a cascade of convolutional and pooling layers for EMG feature extraction, consisting of five processing stages:

Stage 1: The input is the raw EMG signal matrix. A single convolutional layer performs preliminary feature extraction while preserving the temporal characteristics of the original signal.

Stages 2~3: By increasing the number of convolutional kernels (from single-channel to multi-channel), local spatiotemporal features of the signal—such as EMG pulse amplitude and frequency modulation—are progressively extracted. Stacking adjacent convolutional layers deepens the feature representation.

Stages 4~5: Pooling operations are applied to downsample the data, reduce redundancy, and enhance translation invariance, ultimately producing low-dimensional, highly robust abstract feature vectors. These vectors serve as inputs for subsequent fully connected layers for joint-angle regression.

This hierarchical structure, alternating convolution and pooling operations, realizes a progressive mapping from raw EMG signals to high-level motion features, effectively capturing the nonlinear relationship between muscle activity and joint motion.

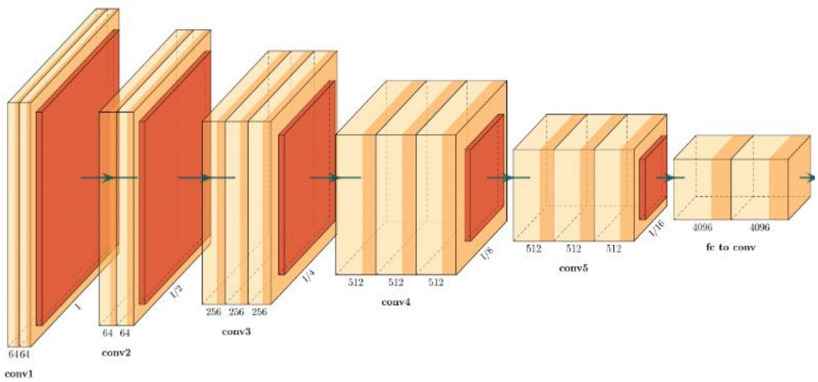

Figure. 13 Schematic diagram of the feature extraction layers in CNN

Figure 14 shows the trends of loss and accuracy for the constructed CNN model over 200 training epochs. In the figure, the green solid line represents training loss, the black solid line represents validation loss, the red dashed line represents training accuracy, and the blue dashed line represents validation accuracy. Detailed analysis is as follows:

Loss function trends: During the initial training phase (epoch 0~25), both training and validation losses decrease rapidly, indicating effective preliminary learning of data features by the model. As training progresses (epoch 25~200), the training loss gradually converges below 0.1, while validation loss remains relatively stable (ranging from 0.15 to 0.3) without significant increase, demonstrating that the model avoids overfitting and exhibits good generalization ability.

Accuracy trends: Training accuracy begins to plateau after epoch 50, stabilizing between 0.85 and 0.9. Validation accuracy increases in parallel and eventually stabilizes around 0.8. The small difference between training and validation accuracy (approximately 0.05~0.1) further confirms the model's sufficient training and reasonable architecture.

These results indicate that the CNN model effectively maps EMG signal features to joint motion estimates through gradient descent optimization, providing a reliable decision-making basis for the exoskeleton control system.

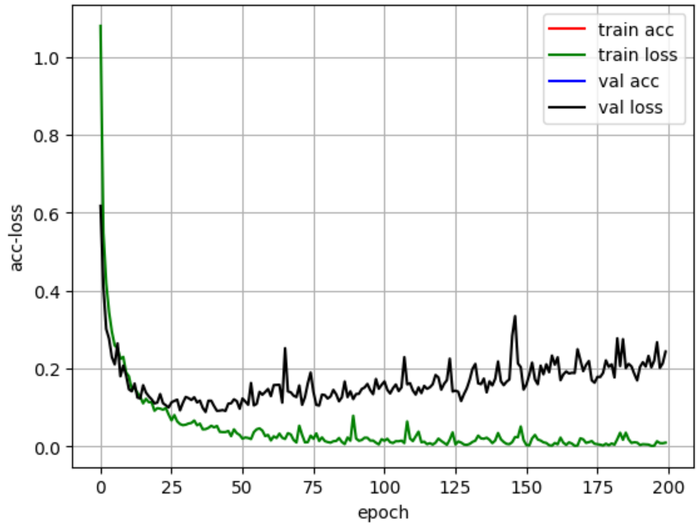

Figure. 14 Neural network training process

3.4. Device Assembly

Figure 15 illustrates the hardware deployment and debugging workflow of the exoskeleton system. First, mechanical components are assembled according to the design schematics, including the elbow rotation module, differential actuation module, and drive system, ensuring that joint ranges of motion and degrees of freedom meet design specifications.

Next, a data communication link is established between the sEMG sensors, motion control card, and host PC via serial interfaces such as USB or CAN bus, with protocol parameters configured to ensure stable data transmission.

Subsequently, electrode placement is tested by attaching surface EMG electrodes to the target muscle bellies (e.g., biceps brachii, brachioradialis) according to anatomical landmarks, with the reference electrode placed on the olecranon of the ulna. Electrode–skin contact impedance is verified using an impedance tester (<5 kΩ), followed by sensor calibration, including signal path verification, filter parameter setup (20~500 Hz band-pass), and baseline noise calibration.

Finally, the data acquisition system is activated to record EMG signals during both resting and dynamic motion states. After verifying signal quality, the system is ready for formal experimental procedures.

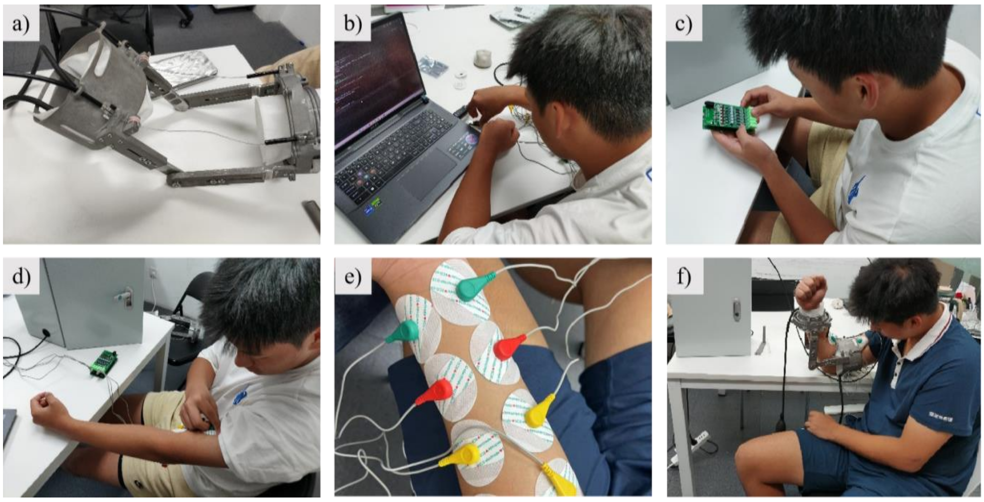

Figure. 15 Hardware deployment and testing workflow: (a) Assemble the exoskeleton device according to design schematics; (b) Connect USB and CAN bus interfaces; (c) Calibrate the EMG sensors; (d) Test electrode signals from target muscles; (e) Install electrodes on the arm; (f) Wear the exoskeleton device

4. Experimental Design

4.1. Subjects and Conditions

This study recruited four healthy male participants (age 22~30 years, height 170~185 cm, weight 60~75 kg), all with no history of upper-limb motor dysfunction or neuromuscular disorders. All participants underwent standardized movement training to ensure stable execution of the prescribed elbow flexion–extension and forearm pronation–supination motions. Two testing modes were employed:

1) Free mode: Participants performed voluntary movements without wearing the exoskeleton.
2) Assistive mode: Participants wore the elbow exoskeleton, which provided assistive torque controlled by sEMG signals.

In both modes, standardized load conditions were applied—participants held a 2 kg dumbbell (±50 g tolerance) to enhance activation of target muscles (e.g., biceps brachii, triceps brachii) and improve the signal-to-noise ratio (SNR) of the sEMG signals. Experimental room temperature was maintained at 23 ± 2 °C with 50 ± 5% humidity to minimize environmental effects on sensor stability and muscle activity.

4.2. Experimental Procedure

The experiment consisted of a preparation phase and a movement execution phase:

Preparation phase: Participants sat upright at the edge of a chair with a relaxed posture and feet flat on the floor. They viewed a standardized action demonstration video on the host PC. In a resting state, participants maintained their forearms in a neutral position for 5 s while baseline sEMG signals and joint-angle data were simultaneously recorded as reference.

Movement execution phase: Using a unified motion paradigm, participants held a 2 kg dumbbell and started from full elbow extension (0°). They flexed the elbow at a constant speed of 0.5 rad/s to 90° (±5° tolerance), paused for 4 s, and then extended back to the starting position at the same speed, completing one flexion–extension cycle in 12 s (including pause). Each forearm posture (pronation 0°, neutral, supination 90°) was repeated five times per trial, with each participant completing three trials. A 3-minute rest interval was provided between trials to prevent muscle fatigue.

Throughout the experiment, a motion capture system (100 Hz) recorded joint-angle trajectories, while sEMG signals were collected at 2000 Hz and stored in the host PC database for subsequent algorithm validation and analysis.

4.3. Data Acquisition

sEMG sensors were used to record target muscle activity. Electrodes were placed on the muscle bellies of elbow-related muscles (e.g., biceps brachii, triceps brachii) according to anatomical landmarks, with reference electrodes positioned on neutral sites such as the olecranon of the ulna to ensure effective detection of muscle potentials. The root mean square (RMS) of the EMG signals was analyzed to quantify differences in muscle activation between the free mode and assistive mode.

4.4. Effectiveness Evaluation

To evaluate the effectiveness of the assistive training, the experiment compared EMG signal amplitude changes between the free mode and assistive mode across three forearm postures. Additionally, the effects of different forearm postures on muscle activation levels were analyzed, as well as the performance differences of the assistive mode in each posture.

5. Results and Discussion

5.1. Time-Domain Comparison of Forearm EMG Amplitude in Free and Assistive Modes

Figure 16 illustrates the temporal changes of forearm EMG amplitude over 0~500 s for the free mode (green solid line) and assistive mode (yellow shaded area). Overall, EMG amplitudes in the assistive mode are lower than those in the free mode, indicating that the exoskeleton effectively reduces muscle activation. Both modes exhibit periodic fluctuations, reflecting the dynamic muscle activity during elbow flexion–extension.

In the free mode, signal fluctuations are larger, with peak values approaching 0.6, whereas in the assistive mode, signals are more stable, with peak values around 0.4. This suggests that the exoskeleton's assistive torque may reduce variability in muscle exertion. The high temporal overlap between the yellow shaded area and the green curve indicates that the timing of muscle activity in the assistive mode closely matches that of the free mode, confirming the synchronization of human–robot cooperative movement.

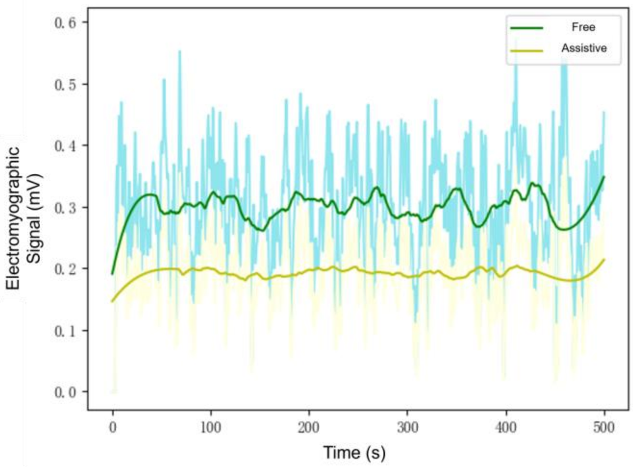

Figure. 16 EMG amplitude variations during assistive training mode

5.2. EMG Signals and Primary Torque Analysis

The RMS of EMG signals, reflecting signal energy, was used to quantify muscle activation levels. The experiment compared RMS distributions of muscles under free mode (no assistance) and assistive mode across different forearm postures (neutral, pronation, supination), as shown in Figure 17, where values represent mean RMS for each muscle in each mode.

Results indicate significant differences in muscle activation across postures and modes:

1) Neutral position flexion: Brachioradialis exhibited the largest RMS change, while triceps brachii showed the smallest, indicating the brachioradialis as the primary force-generating muscle.

2) Pronation flexion: Brachioradialis RMS remained highest, with biceps brachii, triceps brachii, and pronator teres showing lower involvement.

3) Supination flexion: Biceps brachii and brachioradialis RMS changes were prominent, whereas triceps brachii and pronator teres showed smaller changes, highlighting them as the main active muscles.

Table 2 presents the net RMS reduction under assistive mode. Across all forearm postures, RMS values were significantly lower than in free mode, with brachioradialis showing a maximum reduction of 54.76 ± 16.69% and the four upper-limb muscles averaging a 38.53 ± 11.98% decrease. Corresponding primary torque analysis revealed a significant reduction in human-applied torque under assistive mode, with the maximum decrease in supination reaching 66.2 ± 15.34% and an overall average reduction of 58.5 ± 17.27% across postures.

These findings demonstrate that the exoskeleton's assistive control strategy effectively reduces voluntary exertion during elbow flexion by providing precise torque compensation. The results validate the system's assistance to primary muscles and confirm stable human–robot cooperative control.

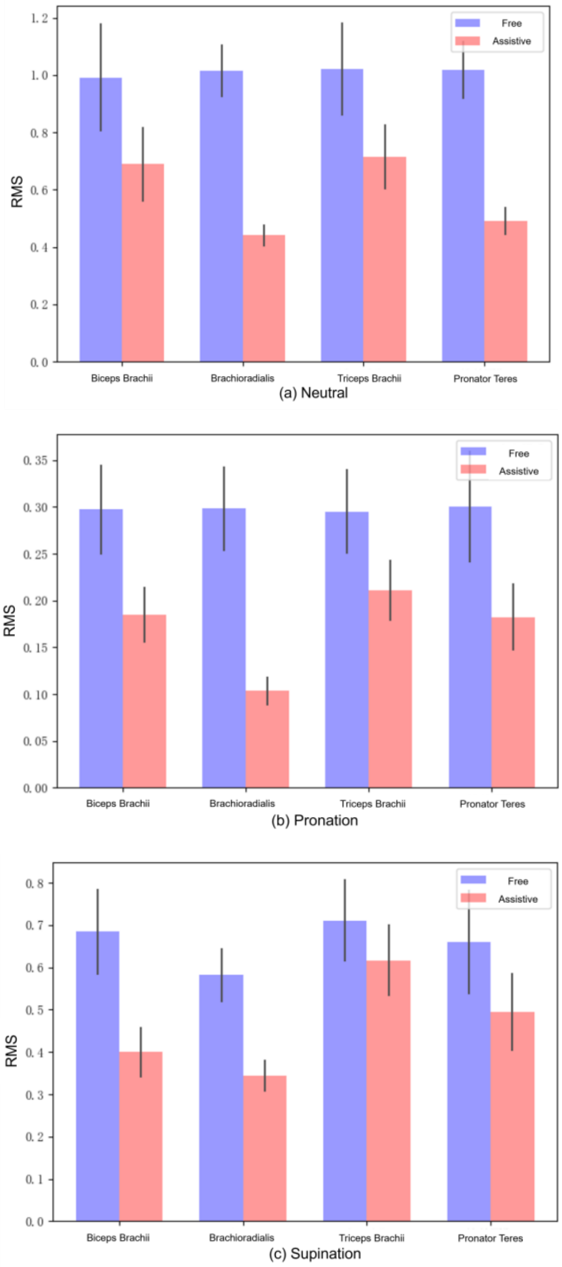

Figure. 17 RMS values of upper-limb muscles

Table. 2 Net RMS reduction rates in assistive mode

Muscle Channel	Net RMS Change (%)
Biceps brachii	~36.8±8.23
Brachioradialis	~54.76±16.69
Triceps brachii	~23.13±10.2
Pronator teres	~39.43±12.8
Average	~38.53±11.98

5.3. Comparison of Net Changes in Human Primary Torque Across Forearm Postures

Figure 18 presents a bar chart distinguishing the contributions of total torque (blue), exoskeleton assistive torque (red), and human-applied primary torque (yellow). Table 3 summarizes the net change rates of human primary torque under assistive mode.

Results indicate that primary torque was significantly reduced across all forearm postures:

Neutral position: ~66.2 ± 15.34%

Pronation: ~57.4 ± 20.55%

Supination: ~52.1 ± 15.93%

Overall average across postures: ~58.5 ± 17.27%

Negative values indicate a substantial reduction of human-applied torque under assistive mode compared to free mode. The greatest reduction occurred in the neutral position, followed by supination, with pronation showing the smallest decrease. These results reflect differences in torque compensation efficiency of the exoskeleton across different forearm postures.

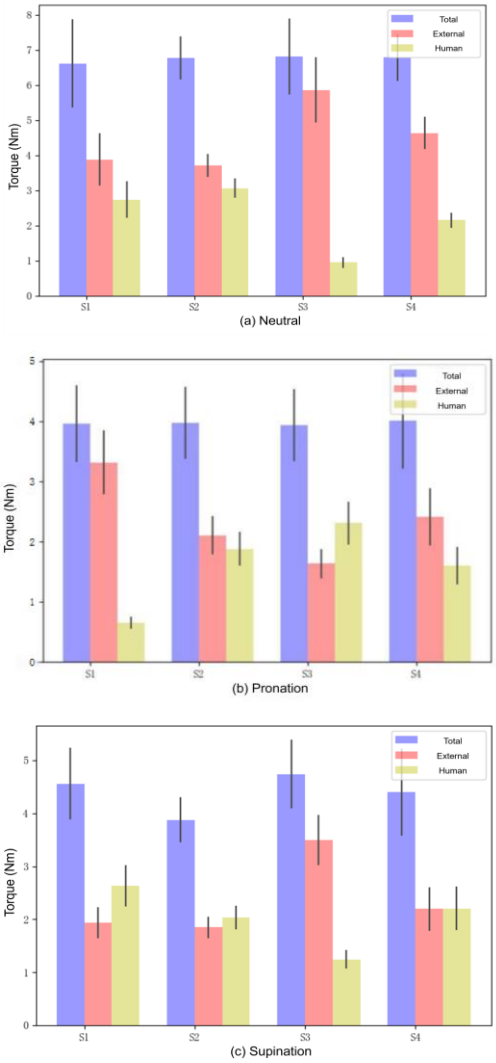

Figure. 18 Torque values of upper-limb muscles

Table. 3 Net change rates of human primary torque in assistive mode

Forearm Posture	Net Change in Human Primary Torque (%)
Neutral	~66.2±15.34
Pronation	~57.4±20.55
Supination	~52.1±15.93
Average	~58.5±17.27

6. Conclusion

The biologically informed elbow exoskeleton rehabilitation device developed in this study integrates an "sEMG → CNN decoding → differential actuation" approach, enabling precise response to human movement intention and compliant assistive torque. The main conclusions are as follows:

Mechanical design: The differential transmission module, controlled by dual motors, achieves decoupled elbow flexion–extension (0°~125°) and forearm pronation–supination (±70°) motions. The structure is compact and meets safety requirements.

Control algorithm: The CNN model effectively extracts spatiotemporal features from EMG signals to estimate joint angles with high accuracy. During training, the loss function converged stably, demonstrating good model generalization.

Experimental validation: Under assistive mode, both muscle activation (RMS) and human-applied primary torque were significantly reduced across three forearm postures. The brachioradialis was the primary active muscle in neutral and pronation positions, while biceps brachii participation increased notably in supination, indicating that the system adapts to different muscle coordination patterns across postures.

Application value: The system reduces average primary torque demand by 58.5% through real-time torque compensation and maintains synchronized human–robot motion timing, providing an intelligent solution for active rehabilitation training in patients with elbow joint dysfunction.

References

[1] Xiong Y P, Zheng C J. Research progress on acupuncture treatment for upper limb motor dysfunction after stroke[J]. Chinese Folk Therapies, 2025, 33(14): 125–128.

[2] Raghavan P. Upper limb motor impairment post stroke[J]. Physical medicine and rehabilitation clinics of North America, 2015, 26(4): 599.

[3] Xuan L Z, Li F F. Research progress on post-traumatic elbow contracture [J]. Chinese Journal of Bone and Joint, 2024, 13(12): 1030–1034.

[4] Chen W, Xiong W W, Gao Q M, et al. Application of MRI in the diagnosis of atypical elbow injuries [J]. Chinese Journal of CT and MRI, 2024, 22(9): 160–162.

[5] Shi W W, Jin L J. Review on research development and clinical application of terminal traction and exoskeleton upper limb rehabilitation robots [J]. Surgical Research and New Technique, 2025, 14(2): 101–106+96.

[6] Jiang J, Huo B, Han Y, et al. Recent patents on end traction upper limb rehabilitation robot[J]. Recent Patents on Mechanical Engineering, 2017, 10(2): 102~110.

[7] Shi J H, Wang N H. Current applications and advances of robotic technology in rehabilitation medicine [J]. Journal of Robotic Surgery, 2024, 5(6): 1154–1166.

[8] Tan R B, Lu S Y, Xu W J, et al. Path planning of upper limb exoskeleton rehabilitation robot based on human-computer interaction [J]. Manufacturing Automation, 2022, 44(11): 58–63.

[9] Schmidt A. Biosignals in human~computer interaction[J]. interactions, 2015, 23(1): 76~79.

[10] Zhang L, Zheng Y X, Xiong T, et al. A scoping review of non-invasive brain-computer interface technology in upper limb rehabilitation for stroke patients and its nursing implications [J]. Chinese Journal of Nursing, 2025, 60(13): 1658–1664.

[11] Wu H B, Chen S G, Jia J. Research progress on brain mechanisms of brain-computer interface technology in upper limb motor function rehabilitation for stroke patients [J]. Journal of Biomedical Engineering, 2025, 42(3): 480–487.

[12] Hasan M M, Aris S A M, Sulaiman N. An overview of electroencephalogram based human~computer interface[J]. Artificial Intelligence and Multimodal Signal Processing in Human~Machine Interaction, 2025: 79~102.

[13] Liang W D, Zhang R, Guo X H, et al. Application value of mirror therapy-based brain-computer interface technology in upper limb rehabilitation of stroke patients[J]. China Medical Device Information, 2025, 31(3): 123-125+158.

[14] Yang N C. Research on joint torque estimation method based on surface electromyography signal and elbow rehabilitation exoskeleton system[D]. South China University of Technology, 2021.